One-Step DNA-Programmed and Flash Synthesis of Anisotropic Noble Metal Nanostructure on MXene

Menglin Song, Yongxin Lyu, Feng Guo, Sin-Yi Pang, Man-Chung Wong, Jianhua Hao*

Department of Applied Physics, The Hong Kong Polytechnic University, Hong Kong, 999077, P. R. China

*Corresponding author. E-mail: jh.hao@polyu.edu.hk

KEYWORDS. 2D MXene, DNA-programmed, rapid synthesis, anisotropic morphology, noble metal nanostructure.

ABSTRACT. Precise morphological control over anisotropic noble metal nanoparticles (ANPs) is one of the key issues in nano research field owing to their unique optoelectronic, magnetic, mechanical, and catalytic properties. Although nanostructures fabricated by directed assembly of adsorbate have been widely demonstrated recently, facile yet universal synthesis of nanocrystal with tunable morphologies, green templates, no seeds and high yield remains challenging. Herein we develop a versatile method, allowing rapid, one-step, seedless, surfactant-free synthesis of noble metal nanostructure with tunable anisotropy on MXene in a sequence-dependent manner through a single DNA molecular regulator. Based on mild reducibility of MXene and selective affinity of the DNA to the specific facets in the crystals, oriented aggregations and growth of ANPs (Au, Pt, Pd) can be achieved and the resulting asymmetric morphology from polyhedrons, or

flowers, or nanoplates, to dendrites. The ability to align such ANPs on the MXene surface is expected to lead to improved photothermal effect and surface-enhanced Raman scattering. Furthermore, our work makes the fabrication of ANPs or ANPs-MXene heterostructure more readily, stimulating further explorations of physical, chemical, and biological application.

INTRODUCTION.

Over the past few decades, the method of fabricating noble nanoparticles with anisotropic morphologies including one-dimensional (1D) materials, two-dimensional (2D) materials and three-dimensional (3D) materials ranging from nanowires[1, 2] nanosheets[3] to polyhedrons[4-7] have garnered vast interest due to their superior properties and potential applications in sensing, electronics, photonics, catalysis, imaging and biomedicine.[8] 3D anisotropic noble metal nanoparticles (ANPs), including star-or flower-shaped nanostructures possess rough surfaces and possible high-index facets that could be complemented in specific surface-sensitive applications such as surface-enhanced Raman scattering (SERS), catalysis and imaging-related application. Despite these fascinating properties, the synthesis of noble metal nanocrystals with well-controlled, three-dimensional, and highly asymmetric structures remains a challenge. Previously, the capping ligands have been the center of interest in regulating the morphology of ANPs. For example, cetyltrimethylammonium bromide/chloride (CTAB/CTAC),[9] polyvinylpyrrolidone (PVP),[10] citrates[11] and halide ions (Br⁻)[12] are conventional capping agents that play a vital role in binding to specific facets (111) or (100) of noble metal (NM), influencing precursors reduction and diffusion as well as providing overall stability. However, these surfactants suffer from some limitations, such as lack of systematic variations and concise tuning of their morphology, the effect of charges and functional groups on the formation of the structure, and toxicity and environmental

risks.[13, 14] To address these issues, many researchers resort to biomolecules (such as amino acids, protein, nucleic acid etc.) as green agents for synthesizing nanomaterials. Among them, DNA with tunable functional groups, charges, affinity and length shows enormous potential in various fields.[15] Because of its well-defined molecular structures and conformations that are predicted from the four-letter genetic codes, DNA is an exceptionally attractive class of capping ligands which can accurately regulate the morphology of nanoparticles by systematic variations and fine-tuning of their structure, charge, or functional groups during the fabrication process [16, 17] In spite of their great success, all the DNA-programmed synthetic schemes for morphological control involve seed-mediated synthesis, which is often monotonous and not conducive to the further exploration of new applications. In addition, the seeds need to be presynthesized, resulting in complicated and time-consuming process for ANPs preparation. Therefore, a facile process for fabricating ANPs or ANPs-integrated composites in one step with synergistically enhanced properties is highly anticipated.

MXenes are one of the latest additions to the family of two-dimensional (2D) materials, comprising transition metal carbides and nitrides produced by selective etching from their parent 3D precursors, the so-called $M_{n+1}AX_n$, (MAX) phases, where M is a transition metal, A represents the element from the group 13 and 14 of the periodic table and X is carbon or nitrogen element (n = 1, 2, or 3), respectively. MXene has emerged as a promising earth-abundant candidate for large-area catalytic energy storage and conversion due to its unique properties of hydrophilicity, high metallic conductivity, and ease of production by solution processing.[18] Thanks to its 2D morphology, large surface to volume ratio and excellent hydrophilicity, MXene is also considered to be an ideal platform for building heterostructures or nanocomposites for diverse areas such as ultrafast photodetectors,[19] efficient catalysts,[20, 21] sensitive electrochemical or gas sensors,[22, 23]

3

excellent photothermal conversion[24] and Raman signal enhancers.[25] These MXene-based heterostructures exhibit significantly enhanced activities and stability, surpassing the sum of their individual components, on account of synergistic coupling between MXene and the secondary materials.[26, 27]

One type of such heterostructure is noble metal (e.g. Ag, Au, Pt, Pd) nanocrystals-MXene hybrid, which performs multiple functions in different fields such as a large-area electronically conductive carrier,[28] Raman spectroscopy signal enhancer,[29] photothermal provider[30] and cocatalyst.[31, 32] The fabrication protocols of these MXene hybrids primarily rely on electrostatic self-assembly and self-reduction stabilization. Among them, *in situ* synthesizing inorganic nanomaterials on MXene is advantageous because the second material is tightly integrated with MXenes, forming a hybrid interface. The ability to align such anisotropic noble metal nanostructures on the MXene surface is expected to lead to the improved functionalities. The anisotropic morphologies of NM mediated by MXene are unexplored. Hence, the ability to precisely control the morphologies (such as shape and surface structure) of NM on MXene, is a key to realize their great potential in a myriad of applications.

Herein, we proposed a DNA-mediated method that enables the fast, one-step, seedless, surfactant-free synthesis of noble metal nanostructure with tunable morphology at room temperature. By moderate reducibility of MXene and precise modulation of DNA, the gold nanostructure with different anisotropy can be tailored. Taking full advantage of the combination of desirable properties, MXene/anisotropic Au hybrids are anticipated to show profoundly enhanced photothermal performances and SRES effect beyond the sum of their individual components. This strategy may not only offer a technological synthesis of anisotropic Au NPs, but

also provide a universal and extendable fabrication process to other noble metal structures, such as Pd nanoplates, nanodendrites, and Pt nanorings.

Given that chemical and physical properties, including optical, electronic, magnetic and catalytic performance, are sensitive to the shape and size of nanocrystals, it is of great necessity to develop synthetic methods to control the morphology. With a combination of properties such as excellent catalytic and optical properties of anisotropic NM nanoparticles, stable and easily tunable microstructure, high electrical conductivity, large chemically active surface, and adjustable hydrophilicity of low dimensional MXenes, these MXene-based heterostructures have great potential, especially in catalysis, energy conversion/storage, and biomedical applications.

RESULTS AND DISCUSSION

ssDNA-mediated controllable synthesis of anisotropic Au nanostructures. The MXene-Au nanoflower were synthesized through a flash DNA mediated synthesis method. Herein, we selected the length of the DNA strand to 30 nt since it has previously been demonstrated that this length may produce nanoparticles with a customized shape and high colloidal stability.[17] Furthermore, it was found that growing nanoparticles in the presence of varied lengths of oligonucleotides produced similar morphologies, indicating that the oligonucleotide sequence, rather than the length, is crucial in morphology regulation. However, in order to preserve the colloidal stability of nanostructures with desired morphology, the oligonucleotides should be more than five bases.[33] The schematic diagram of the crystallization of DNA tailored Au nanostructures on MXene at different growth periods is exhibited in **Figure 1a.** In the typical synthesis process, 3 μM poly A30 was first vortexed with $Ti_3C_2T_x$ MXene (200 μg/mL) suspensions for better adhesion, and then $HAuCl_4$ (25 mM) solution was added into the mixture for anisotropic growth without addition of any other surfactants at room temperature under different periods of time. Longer growing period

allows for the accumulation of more Au nanoclusters on the single-stranded DNA (ssDNA), forming 3D nanoflowers (NF) in 2 min (Figure 1b) and sea urchin-like nanoparticles in 5 min Crystallinity and lattice present in MXene-Au NF_A30 were determined by high-resolution TEM (HRTEM), SAED and XRD. Figure 1c presents the HRTEM images of MXene-Au NF and discloses lattice fringes of 2.35Å, corresponding to the Au (111). The SAED result is shown in Figure 1d, and weak spots (boxed) are indexed as the allowed {200} Bragg reflections, corresponding to a lattice spacing of 0.204 nm. Strong spots (circled) are indexed as the {111} reflections, corresponding to a lattice spacing of 0.235 nm, while the spots (triangle) are indexed as {222}, corresponding to a lattice spacing of 0.107 nm. A typical XRD scan of a few-layered MXene-Au nanoflower powder sample obtained by poly A30 mediation and the reducibility of MXene. Peaks at $2\theta=37.6°$, $43.9°$, $64.2°$ and $77.16°$ can be observed due to 111, 200, 220 and 311 reflections, respectively (Figure 1e). The color of mixture containing A30 is dark blue (Figure S1), and the absorption peak coincides with the original characteristic peak of MXene at 806 nm, demonstrating the formation of Au nanoflowers or nanourchins (Figure 1f). In contrast, the reaction solution without oligonucleotides appears reddish-brown and has a characteristic absorption peak of Au nanosphere at 596 nm. MXene-Au nanoflower has a high plasmonic peak in the NIR range, resulting in enhanced photothermal effect and outstanding SRES activity. Compared with MXene-Au nanospheres, MXene-Au nanoflowers have higher light-to-heat conversion efficiency (Figure S19), which is attributed to the stronger absorption of Ti_3C_2-Au nanoflowers at 808 nm. Besides, the SERS enhancement factor is $2.4x10^4$ when methylene blue solution (1.0×10^{-5} M, 20 μL) is cast on the $Ti_3C_2T_x$-Au nanoflower substrate (Figure S20).The XPS spectra of MXene-Au NF evidenced the presence of Ti, Au and P (Figure 1g). Hence, these findings indicate that poly A30 *in situ* tailored fabrication of Au nanoflowers on MXene.
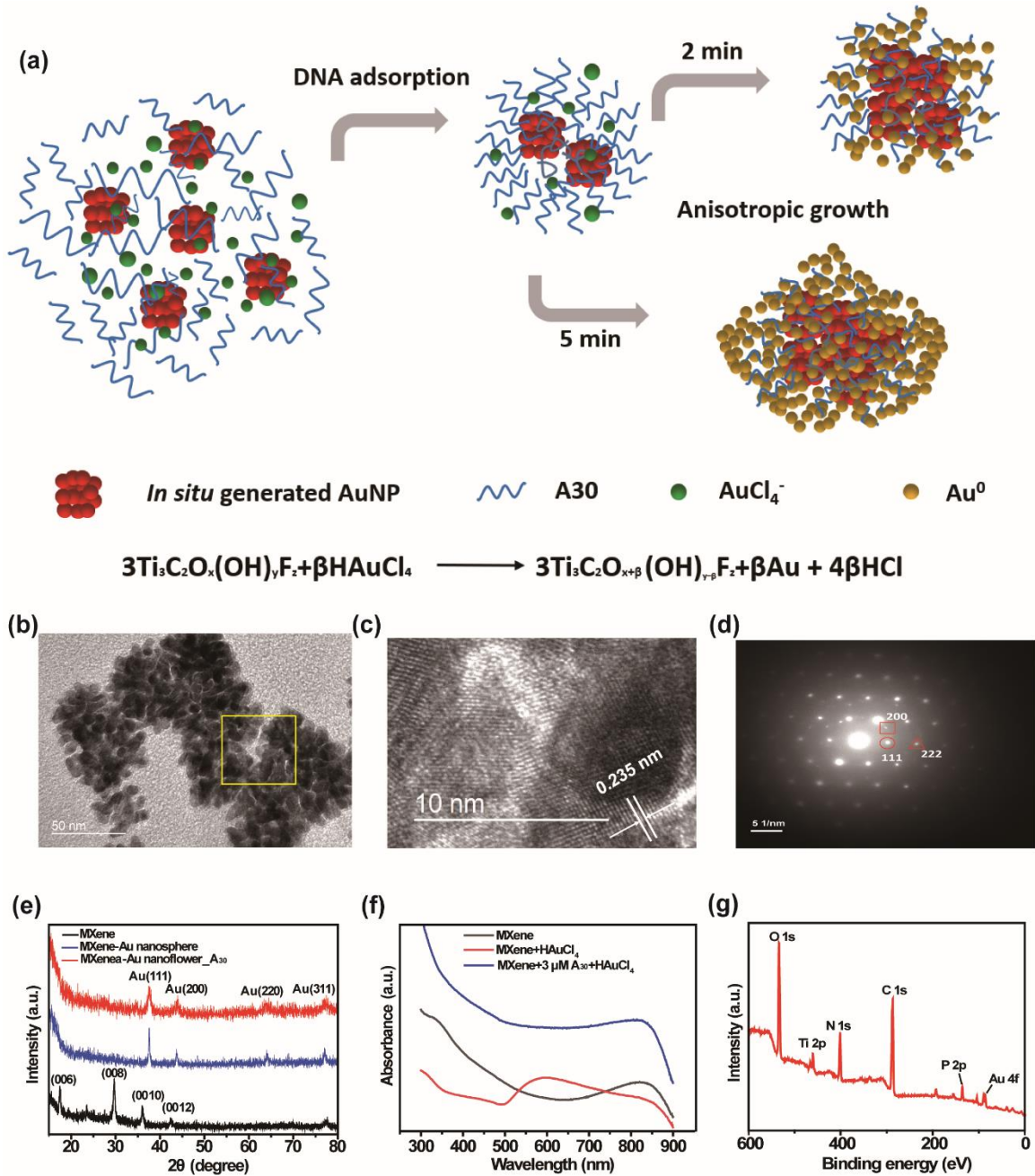
Figure 1. (a) The schematic illustration showing DNA-tailored crystallization of Au nanostructures at different growth time. (b) TEM of PolyA30 mediated *in situ* reduction of Au nanoflower on MXene in 2 minutes. (c) HRTEM of the area outlined by the yellow square in (b). (d) Selected area electron diffraction (SAED) of MXene-A30-Au nanoflower. $Ti_3C_2T_x$ MXene: 0.2 mg/mL, A30: 3 µM, $HAuCl_4$: 25 mM. (e) The powder X-ray diffraction patterns of delaminated

MXene (black line), MXene-Au nanosphere (blue line); MXene-Au nanoflower (red line). (f) UV-vis absorption measurement of MXene incubated with A30 oligonucleotides and HAuCl4. (g) XPS spectrum of MXene-Au nanoflower.

It is well noted that ssDNA can be absorbed onto the gold surface in a sequence-dependent manner. Based on previous studies, dA (adenine) dC (cytosine) and dG (guanine) showed a much stronger binding affinity to gold surfaces than dT (thymine)[34]. This property has been implemented to synthesize varied DNA-templated gold nanostructures or in DNA-based applications. However, DNA-mediated morphological control of different types of ANPs on 2D materials in the absence of seeds has not been studied. This method shows advantages of no seeds, no surfactants, in-situ reduction, and rapid synthesis at room temperature. The process of controlled growth of asymmetric Au nanocrystals is illustrated in **Figure 2a**. Herein three types of 30-mer DNA were selected, including poly A30, poly C30 and poly T30 to investigate the growth of gold nanostructures. MXene is an emerging 2D material (Figure 2b) that possesses high reducibility, surface to volume ratio and excellent hydrophilicity. Therefore, it is regarded as a superb substrate for the synthesis of various metal nanostructures. The resulting nanostructures in MXene suspensions mixed with HAuCl4 solution without addition of any other surfactants are mostly spherical or quasi-spherical (Figure 2c) with the particle size of 42 nm (Figure S2a). To *in situ* manufacture anisotropic noble metal nanostructures, MXene suspensions were incubated with four types of polymeric DNA A30, C30, T30, respectively. G30 was not verified here owing to the complexity of manufacturing oligos with more than 20 consecutive dG bases. Finally, HAuCl4 solution (20 mL, 25 mM) was introduced into the mixture, aiming at providing gold precursor and absorbing DNA molecules. Surprisingly, the resultant solutions in the presence of DNA sequences were dark blue colored, and the anisotropic Au NPs have a broad surface plasmonic absorption

that peaks at 814 nm (A30-1 µM), 816 nm (A30-3 µM),728 nm (C30-1 µM), 820 nm (C30-3 µM), 664 nm (T30-1 µM), 704 nm (T30-3 µM), which indicates that the morphology of gold nanoparticles changes in the presence of DNA (Figure S3). As shown in Figure 2d, and Figure S4a, flower-shaped gold nanoparticles were formed with the presence of 1 µM A30, C30 DNA molecules. The particle size is around 60 nm (for Au NF_A30) or 65 nm (for Au NF_C30). Whereas it becomes urchin-shaped morphology when the concentration of A30 is increased to 3 µM (Figure 2e). Interestingly, the nanoparticles produced by the regulation of 1 µM T30 are diamond-shaped with a particle size of 36 nm (Figure 2f and Figure S2d). When the concentration of T30 reached 3 µM, petal-like nanostructures with high yield were formed on the MXene, which seemed to be assembled from several diamond-shaped nanoparticles as shown in Figure 2f (Figure 2g). T30 will bind to a particular facet of nanocrystallites, which will cause the nanocrystals to assemble and grow into anisotropic nanostructures. When the concentration of ssDNA is raised further, these generated diamonds are assembled through the specific adsorption between DNA and Au, forming petal-like nanostructures. Moreover, Figure 2h-2l show the element distribution including Ti, C, Au and P on the MXene-Au_NF and further elucidate that DNA-mediated Au nanoflowers were successfully synthesized on MXene.
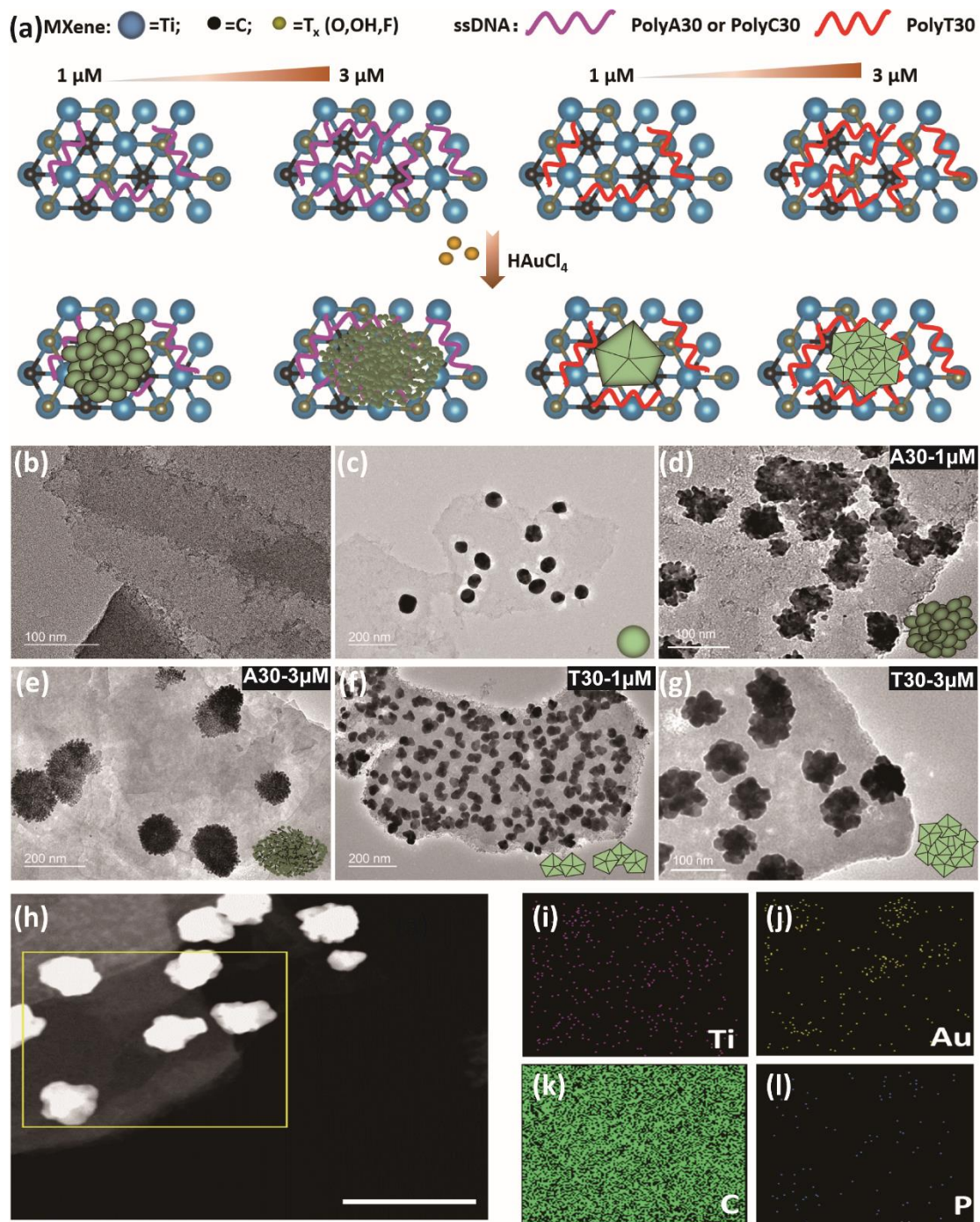
Figure 2. (a) Schematic illustration of DNA-programmed Au nanostructure growth on $Ti_3C_2T_x$. (b) Transmission electron microscopy (TEM) image of $Ti_3C_2T_x$ MXene nanosheet. (c-g) Representative TEM images showing the dependency of the size and anisotropy of Au nanostructure without (c) and with the concentration of 1μM or 3 μM oligonucleotide. (d) A30-

1μM, (e) A30-3μM, (f) T30-1μM, (g) T30-3μM. (h) High-angle annular dark-field scanning transmission electron microscopy (HAADF-STEM) and EDS-STEM of the area outlined by the yellow rectangle. Scale bars are 300 nm. (i-l) the elemental mapping for Ti, Au, C and P of MXene-Au nanoflower.

Kinetics of MXene-mediated Au growth. Diverse nanoplatforms composed of 2D materials with DNA have been utilized for various biosensing applications.[35] Nevertheless, different 2D materials possess disparate surface properties. Specifically, graphene oxide (GO) absorbs DNA or RNA molecules using π-π stacking and hydrogen bonding. In terms of transition metal dichalcogenides (TMDCs) such as molybdenum disulfide (MoS_2), it mainly relies on van der Waals interaction.[36] However, DNA absorption by MXene has been rarely studied previously. It is worth mentioning that MXene carries many negatively charged functional groups (-OH, -F and -O-), which is not favorable for DNA adsorption due to the electrostatic repulsion. Given the above-mentioned facts, it is speculated that the addition of polyvalent metal ions could contribute to promoting DNA oligonucleotides adsorption on unmodified $Ti_3C_2T_x$ MXene. To verify this hypothesis, DNA-MXene interaction was evaluated with fluorescence spectroscopy by incubating the MXene with FAM (6-carboxy fluorescein)-ssDNA. Figure S5 shows the broad absorption spectrum of $Ti_3C_2T_x$ overlaps the emission peak of the FAM dye. Forster resonance energy transfer (FRET) is envisioned to take place owing to the proximity of the FAM covalently bound to one end of ssDNA, to the surface of the $Ti_3C_2T_x$, causing fluorescence quenching (Figure S6). Figure S7 depicts the fluorescence kinetic profiling of FAM-ssDNA treated with MXene for 60 min. The fluorescence emission of the sample was measured in time-resolved experiments, and the quenching efficiency for the FAM in the presence of MXene was determined to be around 65%.

11

As shown in **Figure 3a,** not all the ssDNA sequences were absorbed on the MXene owing to the repelling force between highly electronegative surface groups on MXene and the phosphate backbone of DNA. In contrast, FAM-A30 was tightly bound to MXene after the introduction of HAuCl$_4$ solution. The fluorescence intensity of the supernatants at 520 nm decreased sharply, suggesting DNA oligonucleotides were tightly adsorbed on Ti$_3$C$_2$T$_x$ MXene nanosheet with the assist of the Au^{3+} that seems like a linker connecting MXene and DNA, which greatly promotes DNA adsorption and plays a vital role in morphological tunability. Moreover, Figure 3b also verified this result that Au^{3+} could fully neutralize the MXene surface, Au^{3+} adsorbed on the Ti$_3$C$_2$T$_x$ MXene significantly reducing the charge repulsion between the DNA and MXene. It is worth mentioning that adsorbed ssDNA may be desorbed in the presence of denatured or competitive or chemicals, resulting in fluorescence enhancement. Or the introduction of certain metal ions may also enhance the adsorption capacity of DNA due to the stronger interaction between metal ions and DNA and MXene. As a result, it is critical to exclude additional salt sources as well as acidic or basic environment when using this DNA-mediated approach to control the morphology of Au nanoparticles (Figure S8). Having established the Au^{3+}-mediated DNA absorption effect, we then evaluated the kinetics of A30-mediated Au growth through the visible absorption spectra and TEM observation. In the first 1 min, the absorption from 500 nm to 800 nm increased dramatically (characteristic of plasmonic nanostructures), showing that the kinetics of Ti$_3$C$_2$T$_x$ MXene-mediated Au nucleation and growth with anisotropy is rapid even at room temperature. Along with the growth time, the absorption strength remains basically unchanged, suggesting the formation of larger-sized Au structures has reached saturation (Figure 3c). These results agree with the observations under TEM in Figure 3d-f, which have shed a light on how the nucleation and growth of small nanocrystallites. The nanocrystalline assembly tailored by A30 can

be completed in only 2 min, indicating that the size of the Au nanostructures grew ultrafast. Poly A30 possesses the highest binding affinity to Au atoms and is able to stabilize the surface of Au with higher energy to facilitate the nanocrystallites formation that eventually coalesce into bigger particles, favoring an anisotropic shape. These results together demonstrate that the MXene enables Au growth with fast kinetics. Based on these observations, we envisioned the DNA-mediated gold nanoflower formation process on MXene in Figure 3g. Au^{3+} plays a vital role as a bridge that connects $Ti_3C_2T_x$ and DNA oligonucleotides, and it also provides an essential metal source and is reduced *in situ* into anisotropic nanostructures on MXene under the customization of DNA sequence.

To better understand the influence of ssDNA on the morphology of Au nanostructures, we next used varied concentrations of ssDNA to react with MXene. It was found that the anisotropy of Au nanoparticles increased with the rise of the A30 concentration. The asymmetric morphology from polyhedrons to nanoflowers (Figure S10). More Poly A30 with high affinity will be attached to the facet of small Au nanoseeds with enhancement of ssDNA concentration, resulting in the assembly of nanocrystallites to grow into anisotropic nanostructures. Interestingly, only spherical particles can be generated when a $HAuCl_4$ solution is added to the MXene suspension prior to the addition of the ssDNA solution. (Figure S11). Furthermore, the ratio of MXene and $HAuCl_4$ is shown less effect on the morphology of resultant hybrid nanostructure. As shown in Figure S12, the higher the Au/Ti ratio, the stronger the absorption of Ti_3C_2-Au nanocomposite in the NIR-I region. The absorbance at 808 nm of nanocomposites was approximately 1.25 times than that of Ti_3C_2 nanosheets when the Au/Ti ratio was raised to 3:8. However, the characteristic peak at remained unchanged. All these results indicate that the presence of ssDNA have a stronger influence on the control of Au NPs morphology, rather than the ratio of Au/Ti_3C_2.
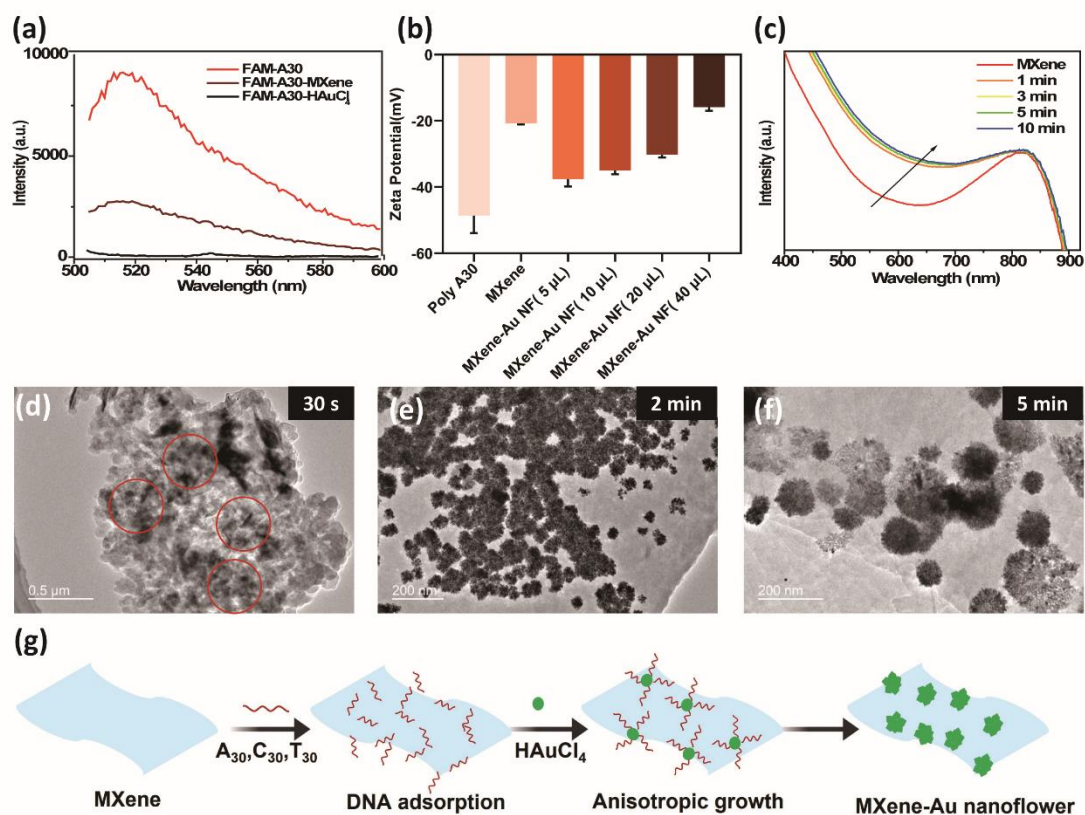
Figure 3. Kinetics of MXene-mediated Au growth. (a) The photoluminescence intensity of the supernatant of each solution after centrifugation: FAM-A30, MXene/FAM-A30 and MXene/FAM-A30 suspension with addition of $AuCl_4^-$, (λ_{ex}=490 nm, λ_{em}=520 nm, $C_{FAM-A30}$= 3 μM, C_{MXene}=200 μg/mL). (b) Zeta potential of polyA30, $HAuCl_4$, MXene and MXene-Au nanoflower with addition of different concentration of $HAuCl_4$ aqueous solution. (c) Kinetics of the visible absorption spectra (400−900 nm wavelength, 0−10 min). (d-f) Typical TEM images (left) of the Au nanoflowers (right) from different growth time (30s, 2 min, and 5 min). (g) The presentative schematic illustration of the synthesis of Au nanoflower on multilayer MXene.

Density functional theory (DFT) calculations between MXene and noble metal (Au, Pd, Pt) atoms. To unveil the mechanisms behind this ultrafast growth of Au anisotropic nanostructures on $Ti_3C_2T_x$, density functional theory (DFT) calculations were conducted to analyze the interaction between Au atoms and MXene. The initial structures of Au/different terminated $Ti_3C_2T_x$ MXenes were fully relaxed. Considering the close-packed stacking order, the upper metal atom may locate at two different sites, either on top of the nearby Ti atom (stacking mode A, Figure S14a) or on top of the nearby C atom (stacking mode B, Figure S14b). By comparing the ground state energy of the two structures, we found that the stacking mode A was more energetically favorable than the stacking mode B for all kinds of functional groups and metal atoms. We therefore conclude that this stacking site (mode A) is likely to be the starting point for metal growth. The optimized structure data for the most stable configurations (i.e., stacking mode A) are listed in table S2 and S3. After the deposition of metal on MXene surface, the bonding between the uppermost Ti and the nearby functional group on this surface experienced different degree of shortening (Table S2); while the bond length on the other surface barely changed. It implies that the interaction of the deposited metal layer with the original MXene layer. Figure 4a shows the side and top views of the most stable molecular configuration for Au atoms on $Ti_3C_2(OH)_2$ through DFT simulations the vertical equilibrium distance between Au atoms and -OH is about 1.867 Å. The vertical distance among all combinations of metal was concluded in the Table S3 and functional groups falls in the range of 1.6 ~ 3.2 Å, with a downward trend in the sequence of -F, -O, -OH. The average distances are much shorter comparing to that of Au-graphene binding (~4 Å) and Au-graphdiyne binding (~3 Å), implying a much stronger binding interaction in our sample.[37] Figure 4b exhibits the binding energy between metal atoms and MXene layers. In consistence with the trend of structure parameters, the OH-terminated group shows strongest binding energy while F-terminated group

has the weakest binding interaction. This phenomenon may be explained by the decrease of electronegativity in the order of F, O, H, which in very good agreement with previous calculations on the adsorption of gas at different terminated MXene.[23] These simulation results elucidate that the super-fast growth of the metal nanostructures on MXene may be ascribed to the high binding energy and close proximity between the Au and MXene.
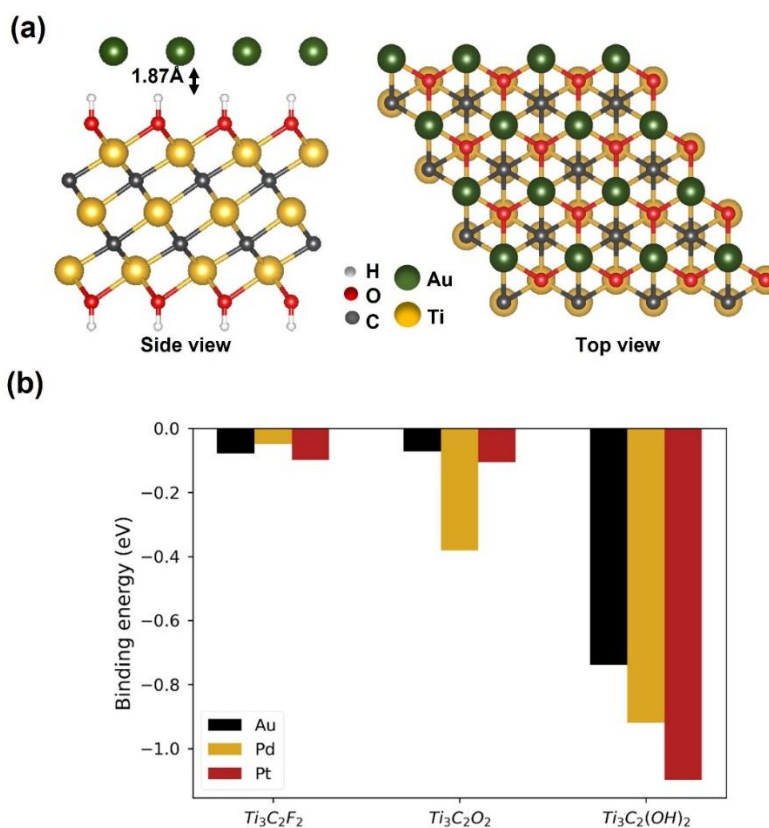

Figure 4. (a) Side and top views of minimum energy configurations for Au atoms adsorbed on surface based on DFT simulations. (b) Calculated minimum binding energies of noble metal atoms on different terminated $Ti_3C_2T_x$.

***In situ* preparation of other anisotropic noble metals nanocrystal on MXene.** Having established that the properties of $Ti_3C_2T_x$ MXene surface play a critical role in the formation of

ANPs by the DFT simulation, it is reasonable to hypothesize MXene could also be used as nanoreactors for the reduction of other noble metals. To testify this hypothesis and explore whether the morphology of nanostructure could also be tailored by different DNA sequences. We here designated tetrachloropalladate acid and chloroplatinic acid as the respective precursors of Pd and Pt nanoparticles. Its manufacturing process is similar to that of fabricating anisotropic MXene-Au nanostructures, and the details are depicted in the method and materials. The morphology of Pd NPs or Pt NPs was also assessed by TEM. As shown in **Figure 5a**, planar Pd nanoplates with good uniformity can be formed by simply mixing MXene suspensions with H_2PdCl_4 aqueous solution. The atomic force microscope (AFM) image in Figure S16 shows that the typical thickness of the Pd nanoplates is around 7.6 nm. The introduction of the C30 or T30 DNA sequences, which can bind strongly to specific facets of Pd nanocrystals, leading to a diverse increasing ratio of different facets in determining the morphology and size of Pd decahedrons (Figure 5b). Interestingly, the dendrites liked structure extending throughout the Pd nanoparticles were observed on MXene for the introduction of the Poly A30 (Figure 5c). Owing to the strong affinity between A30 and Pd, substantial A30 molecules could be absorbed on the MXene through the bridge connection, which destroys the flatness of the substrate, causing uneven distribution of nucleation sites and irregular morphologies. Furthermore, HR-TEM was also employed, demonstrating the dendrites-liked Pd nanoparticles had a very rough fractal-like surface which is preferable for electrocatalysis.[38] Lattice fringes with an interplanar spacing of 2.40 Å, corresponding to 1/3(422) fringes of fcc palladium, are observed in the HRTEM image of an individual nanodendrites (Figure 5d). The reflection was also confirmed by the XRD result in Figure 5g. The element mapping and point-mode energy-dispersive X-ray (EDX) analysis indicate that the MXene-Pd nanodendrites consisted of Ti, C, P and Pd, suggesting the existence of oligonucleotide (element P) and the

17

formation of Pd nanodendrites (Figure 5e, f and Figure S17). Apart from that, XPS scan further verified that DNA was successfully tethered on the MXene and evidenced that it could mediate (Figure 5h, i, j) the Pd nanoparticle growth with anisotropy. More importantly, this universal DNA-tailored strategy can also be applied for the fabrication of anisotropic platinum nanostructures. As illustrated in Figure 5k, Pt nanorings was precisely tailored by poly A30 on MXene. Based on the unique properties of asymmetric structure, we strongly believed that the MXene-Pt nanorings hold a great potential in varied application in the future.
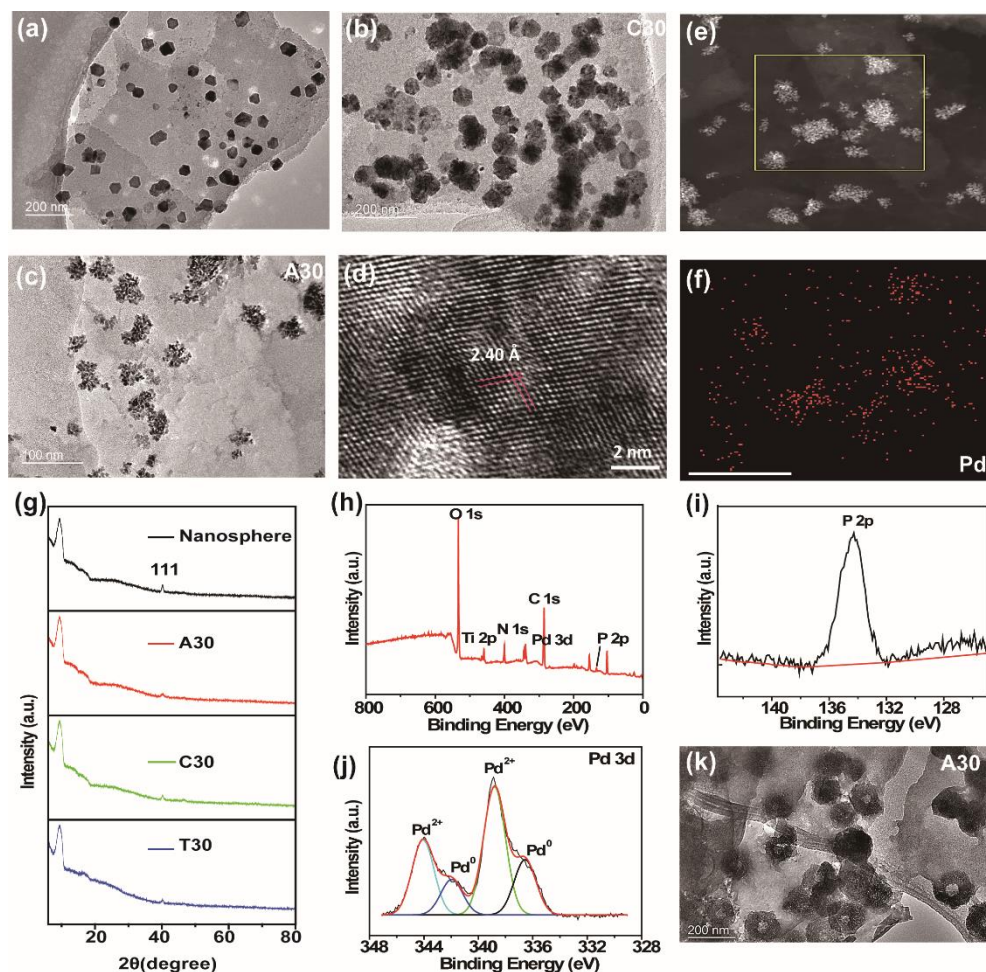

Figure 5. *In situ* synthesis of Pd nanostructure on MXene: (a) TEM image of *in situ* synthesis of Pd nanoplates on MXene (b) MXene-Pd nanodendrites tailored by A30 and (c) MXene-Pd

decahedrons tailored by C30. (d) HRTEM of MXene-Pd nanodendrites tailored by A30. (e) HAADF-STEM of A30 mediated Pd nanodendrites on MXene. (f) EDS-STEM of the area outlined by the yellow rectangle in (e). Scale bars are 300 nm.(g) The powder X-ray diffraction patterns: MXene incubated with H_2PdCl_4 and A30, C30 or T30, respectively. (h) XPS survey of MXene-Pd nanodendrites and high-resolution deconvoluted spectrum on (i) p 2p and (j) Pd 3d. (k) TEM image of MXene-Pt nanorings tailored by A30.

CONCLUSION

In this study, we proposed a universal DNA-mediated synthesis of asymmetric noble metal nanostructures with excellent tunability on MXene. This ssDNA-customized fabrication strategy exhibits several noteworthy features: 1) Facile methodology with rapidity. In previous studies, two-steps and seed-mediated methods have been generally conducted to synthesize the ANPs. Here, we have adopted a one-step and seedless synthesis strategy to synthesize noble metal nanostructure with controllable morphologies tailored by different sequences of ssDNA. This method does not require tedious steps, any surfactants and seeds, and allows fast assembly of nanocrystalline tailored by DNA, facilitating flash synthesis of anisotropic noble metal nanostructures in 5 minutes at room temperature. 2) Investigation of the effect of varied ssDNA on the ANPs morphology. The nucleotides have the capability of activating the fabrication of noble metal nanoparticles with anisotropic morphologies at room temperature and may have a response to the plasmonic signal, coupled with friendly environmental properties, endows this nanoplatform has the potential for molecules biosensing. 3) This universal methodology can be expanded to synthesize other anisotropic noble metal nanostructures on MXene, including Pd nanoplates, Pd

19

or Pt nanodendrites, and Pt nanorings. Such unique anisotropy brings about versatile advantageous properties, promoting comprehensive utilization in various fields. 4) Moderate reducibility and large surface area of MXene, making it a good substrate and facilitating to assemble the MXene with other nanomaterials. A great diversity of properties can be achieved using this in situ reduction and mediation strategy. Benefiting from this novel fabrication method and prominent advantages of MXene-ANPs heterostructures, various applications in catalysis, biosensing, nanophotonics, nanoelectronics and theranostics could be explored.

ASSOCIATED CONTENT

Supporting Information.

Detailed experimental methods, additional graphs of nanoparticle shape and size distributions, additional transmission electron microscopy images, the UV-vis absorption measurement of MXene incubated with different types of oligonucleotides and $HAuCl_4$; and AFM images and height profile of Pd nanoplates on MXene. (PDF)

AUTHOR INFORMATION

Corresponding Author

Jianhua Hao - Department of Applied Physics, The Hong Kong Polytechnic University, Hung Hom, Kowloon, Hong Kong, 999077, P. R. China; ORCID: http://orcid.org/0000-0002-6186-5169; Email: jh.hao@polyu.edu.hk.

Authors

Menglin Song - Department of Applied Physics, The Hong Kong Polytechnic University, Hung Hom, Kowloon, Hong Kong, 999077, P. R. China; ORCID: https://orcid.org/0000-0001-6091-0485.

Yongxin Lyu - Department of Applied Physics, The Hong Kong Polytechnic University, Hung Hom, Kowloon, Hong Kong, 999077, P. R. China

Feng Guo - Department of Applied Physics, The Hong Kong Polytechnic University, Hung Hom, Kowloon, Hong Kong, 999077, P. R. China

 Sin-Yi Pang - Department of Applied Physics, The Hong Kong Polytechnic University, Hung Hom, Kowloon, Hong Kong, 999077, P. R. China

Man-Chung Wong - Department of Applied Physics, The Hong Kong Polytechnic University, Hung Hom, Kowloon, Hong Kong, 999077, P. R. China

Author Contributions

All authors have given approval to the final version of the manuscript. M.S. conducted the overall experiments, measurements, analysis, and wrote the manuscript. Y.L. contributed to simulation analysis. F.G. contributed to the measurement of XRD characterization. S.Y.P. and M.C.W. provided the assistance on chemical analysis. J.H. guided the study and supervised the project. All authors discussed the results and commented on the manuscript.

Notes

The authors declare no competing financial interest.

REFERENCES

1.   Kim, F.; Sohn, K.; Wu, J.; Huang, J., Chemical Synthesis of Gold Nanowires in Acidic Solutions. *J. Am. Chem. Soc*. **2008**, 130, 14442-14443.

2.   Si, K. J.; Sikdar, D.; Chen, Y.; Eftekhari, F.; Xu, Z.; Tang, Y.; Xiong, W.; Guo, P.; Zhang, S.; Lu, Y., Giant Plasmene Nanosheets, Nanoribbons, and Origami. *ACS nano* **2014**, 8, 11086-11093.

3.   Huang, X.; Tang, S.; Mu, X.; Dai, Y.; Chen, G.; Zhou, Z.; Ruan, F.; Yang, Z.; Zheng, N., Freestanding Palladium Nanosheets with Plasmonic and Catalytic Properties. *Nat. Nanotechnol.* **2011**, 6, 28-32.

4.   Sánchez-Iglesias, A.; Pastoriza-Santos, I.; Pérez-Juste, J.; Rodríguez-González, B.; Garcia de Abajo, F. J.; Liz-Marzán, L. M., Synthesis and Optical Properties of Gold Nanodecahedra with Size Control. *Adv. Mater.* **2006**, 18, 2529-2534.

5.   Kumar, P. S.; Pastoriza-Santos, I.; Rodríguez-González, B.; De Abajo, F. J. G.; Liz-Marzán, L. M., High-Yield Synthesis and Optical Response of Gold Nanostars. *Nanotechnology* **2007**, 19, 015606.

6.   Skrabalak, S. E.; Au, L.; Li, X.; Xia, Y., Facile Synthesis of Ag Nanocubes and Au Nanocages. *Nat. Protoc.* 2**007**, 2, 2182-2190.

7.   Xie, J.; Zhang, Q.; Lee, J. Y.; Wang, D. I., The Synthesis of SERS-Active Gold Nanoflower Tags for *In Vivo* Applications. *ACS nano* **2008**, 2, 2473-2480.

8.   Song, M.; Liu, N.; He, L.; Liu, G.; Ling, D.; Su, X.; Sun, X., Porous Hollow Palladium Nanoplatform for Imaging-Guided Trimodal Chemo-, Photothermal-, and Radiotherapy. *Nano Res*. **2018**, 11, 2796-2808.

9.   Pérez-Juste, J.; Liz-Marzán, L. M.; Carnie, S.; Chan, D. Y.; Mulvaney, P., Electric-Field-Directed Growth of Gold Nanorods in Aqueous Surfactant Solutions. *Adv. Funct. Mater.* **2004**, 14, 571-579.

10.   Kim, F.; Connor, S.; Song, H.; Kuykendall, T.; Yang, P., Platonic Gold Nanocrystals. *Angew. Chem. Int. Ed.* **2004**, 43, 3673-3677.

11.   Murphy, C. J.; Sau, T. K.; Gole, A. M.; Orendorff, C. J.; Gao, J.; Gou, L.; Hunyadi, S. E.; Li, T., Anisotropic Metal Nanoparticles: Synthesis, Assembly, and Optical Applications. *J. Phys. Chem.* B **2005**, 109, 13857-13870.

12.   Peng, H.-C.; Xie, S.; Park, J.; Xia, X.; Xia, Y., Quantitative Analysis of the Coverage Density of Br–Ions on Pd {100} Facets and Its Role in Controlling the Shape of Pd Nanocrystals. J. *Am. Chem. Soc.* **2013**, 135, 3780-3783.

13.   Cserháti, T.; Forgács, E.; Oros, G., Biological Activity and Environmental Impact of Anionic Surfactants. *Environ. Int.* **2002**, 28, 337-348.

14.   Ray, P. C.; Yu, H.; Fu, P. P., Toxicity and Environmental Risks of Nanomaterials: Challenges and Future Needs. *J. Environ. Sci. Health C* **2009**, 27, 1-35.

15.   Lu, C.; Huang, Z.; Liu, B.; Liu, Y.; Ying, Y.; Liu, J., Poly-Cytosine DNA as a High-Affinity Ligand for Inorganic Nanomaterials. *Angew. Chem. Int. Ed.* **2017**, 56, 6208-6212.

16.   Ma, X.; Huh, J.; Park, W.; Lee, L. P.; Kwon, Y. J.; Sim, S. J., Gold Nanocrystals with DNA-Directed Morphologies. *Nat. Commun*. **2016**, 7, 1-8.

17.   Wang, Z.; Zhang, J.; Ekman, J. M.; Kenis, P. J.; Lu, Y., DNA-Mediated Control of Metal Nanoparticle Shape: One-Pot Synthesis and Cellular Uptake of Highly Stable and Functional Gold Nanoflowers. *Nano Lett.* **2010**, 10, 1886-1891.

18.   Pang, S.-Y.; Wong, Y.-T.; Yuan, S.; Liu, Y.; Tsang, M.-K.; Yang, Z.; Huang, H.; Wong, W.-T.; Hao, J., Universal Strategy for HF-Free Facile and Rapid Synthesis of Two-Dimensional MXenes as Multifunctional Energy Materials. *J. Am. Chem. Soc*. **2019**, 141, 9610-9616.

19.   Velusamy, D. B.; El-Demellawi, J. K.; El-Zohry, A. M.; Giugni, A.; Lopatin, S.; Hedhili, M. N.; Mansour, A. E.; Fabrizio, E. D.; Mohammed, O. F.; Alshareef, H. N., MXenes for Plasmonic Photodetection. *Adv. Mater.* **2019**, 31, 1807658.

20.   Pang, S. Y.; Io, W. F.; Wong, L. W.; Zhao, J.; Hao, J., Efficient Energy Conversion and Storage Based on Robust Fluoride-Free Self-Assembled 1D Niobium Carbide in 3D Nanowire Network. *Adv. Sci.* **2020**, 7, 1903680.

21.   Yuan, S.; Pang, S.-Y.; Hao, J., 2D Transition Metal Dichalcogenides, Carbides, Nitrides, and Their Applications in Supercapacitors and Electrocatalytic Hydrogen Evolution Reaction. *Appl. Phys. Rev.* **2020**, 7, 021304.

22.   Song, M.; Pang, S. Y.; Guo, F.; Wong, M. C.; Hao, J., Fluoride-Free 2D Niobium Carbide MXenes as Stable and Biocompatible Nanoplatforms for Electrochemical Biosensors with Ultrahigh Sensitivity. *Adv. Sci.* **2020**, 7, 2001546.

23.   Kim, S. J.; Koh, H.-J.; Ren, C. E.; Kwon, O.; Maleski, K.; Cho, S.-Y.; Anasori, B.; Kim, C.-K.; Choi, Y.-K.; Kim, J., Metallic $Ti_3C_2T_x$ MXene Gas Sensors with Ultrahigh Signal-to-Noise Ratio. *ACS nano* **2018**, 12, 986-993.

24.   Lin, H.; Wang, X.; Yu, L.; Chen, Y.; Shi, J., Two-Dimensional Ultrathin MXene Ceramic Nanosheets for Photothermal Conversion. *Nano Lett.* **2017**, 17, 384-391.

25.   Soundiraraju, B.; George, B. K., Two-Dimensional Titanium Nitride (Ti_2N) MXene: Synthesis, Characterization, and Potential Application as Surface-Enhanced Raman Scattering Substrate. *ACS nano* **2017**, 11, 8892-8900.

26. Yao Y.; Lan L.; Liu X.; Ying Y.; Ping J., Spontaneous Growth and Regulation of Noble Metal Nanoparticles on Flexible Biomimetic MXene Paper for Bioelectronics. *Biosens. Bioelectron*. **2020**,148, 111799.

27. Zhao F.; Yao Y.; Jiang C.; Shao Y.; Barceló D.; Ying Y.; Ping J., Self-Reduction Bimetallic Nanoparticles on Ultrathin MXene Nanosheets as Functional Platform for Pesticide Sensing. *J. Hazard. Mater*. **2020**, 384, 121358.

28.   Zou, G.; Zhang, Z.; Guo, J.; Liu, B.; Zhang, Q.; Fernandez, C.; Peng, Q., Synthesis of MXene/Ag Composites for Extraordinary Long Cycle Lifetime Lithium Storage at High Rates. *ACS Appl. Mater. Interfaces* **2016**, 8, 22280-22286.

29.   Satheeshkumar, E.; Makaryan, T.; Melikyan, A.; Minassian, H.; Gogotsi, Y.; Yoshimura, M., One-Step Solution Processing of Ag, Au and Pd@ MXene Hybrids for SERS. *Sci. Rep.* **2016**, 6, 1-9.

30.   Tang, W.; Dong, Z.; Zhang, R.; Yi, X.; Yang, K.; Jin, M.; Yuan, C.; Xiao, Z.; Liu, Z.; Cheng, L., Multifunctional Two-Dimensional Core-Shell MXene@Gold Nanocomposites for Enhanced Photo-Radio Combined Therapy in the Second Biological Window. *ACS nano* **2018**, 13, 284-294.

31.   Zhang, J.; Zhao, Y.; Guo, X.; Chen, C.; Dong, C.-L.; Liu, R.-S.; Han, C.-P.; Li, Y.; Gogotsi, Y.; Wang, G., Single Platinum Atoms Immobilized on an MXene as an Efficient Catalyst for the Hydrogen Evolution Reaction. *Nat. Catal.* **2018**, 1, 985-992.

32.   Ran, J.; Gao, G.; Li, F.-T.; Ma, T.-Y.; Du, A.; Qiao, S.-Z., Ti_3C_2 MXene Co-Catalyst on Metal Sulfide Photo-Absorbers for Enhanced Visible-Light Photocatalytic Hydrogen Production. *Nat. Commun.* **2017**, 8, 1-10.

33. Wang Z.; Tang L.; Tan L. H.; Li J.; Lu Y., Discovery of the DNA "Genetic Code" for Abiological Gold Nanoparticle Morphologies. *Angew. Chem. Int. Ed*. **2012**, 51, 9078-82.

34.   Satyavolu, N. S. R.; Loh, K. Y.; Tan, L. H.; Lu, Y., Discovery of and Insights into DNA "Codes" for Tunable Morphologies of Metal Nanoparticles. *Small* **2019**, 15, 1900975.

35.   Song, M.; Yang, M.; Hao, J., Pathogenic Virus Detection by Optical Nanobiosensors. *Cell Rep. Phys. Sci.* **2021**, 2, 100288.

36. Zhu, C.; Zeng, Z.; Li, H.; Li, F.; Fan, C.; Zhang, H., Single-Layer MoS$_2$-Based Nanoprobes for Homogeneous Detection of Biomolecules. *J. Am. Chem. Soc.* **2013**, 135, 5998-6001.

37. Chen, X.; He, F.; Fang, W.; Shen, J.; Liu, X.; Xue, Y.; Liu, H.; Li, J.; Wang, L.; Li, Y., DNA-Guided Room-Temperature Synthesis of Single-Crystalline Gold Nanostructures on Graphdiyne Substrates. *ACS Cent. Sci.* **2020**, 6, 779-786.

38. Iqbal, M.; Li, C.; Jiang, B.; Hossain, M. S. A.; Islam, M. T.; Henzie, J.; Yamauchi, Y., Tethering Mesoporous Pd Nanoparticles to Reduced Graphene Oxide Sheets Forms Highly Efficient Electrooxidation Catalysts. *J. Mater. Chem. A* **2017**, 5, 21249-21256.

Table of Contents
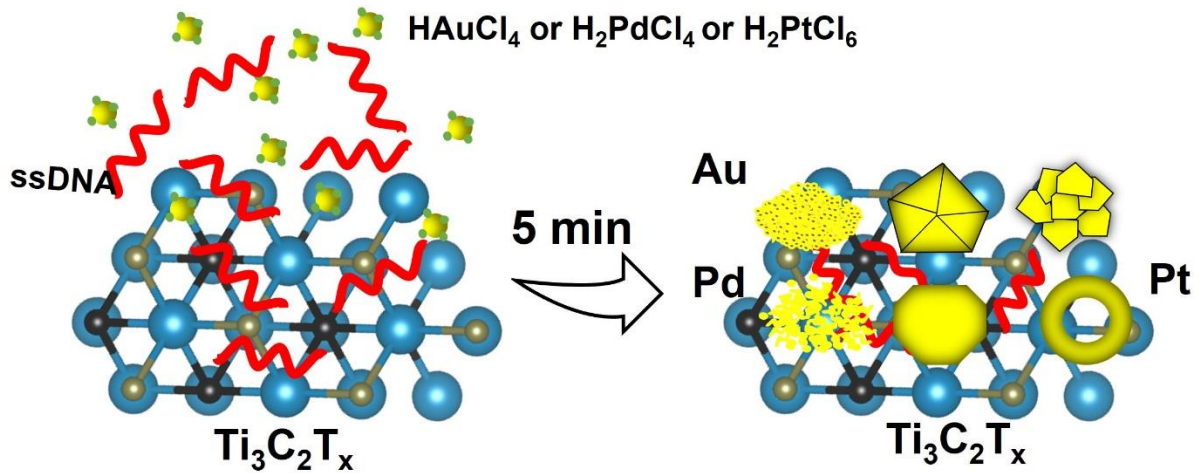
We proposed a DNA-mediated strategy that allows the rapid, one-step, seedless, surfactant-free synthesis of noble metal nanostructure with tunable morphology under room temperature, which also can be extended to fabricate other anisotropic noble metal structures including Pd nanoplate, nanodendrite, and Pt nanoring.